

Supplementary material for Journal of Geophysical Research paper JB2011008711

Resolution Tests

2 1. Ray path coverage

3 Plots of ray coverage ([Figure A4](#)) help identify those parts of the model, which are well
4 resolved. Ray coverage is determined by the geometry of the receivers and sound sources. The
5 plots are binned at source-receiver intervals of 20 km. Using a basic rule of thumb of $\frac{1}{4}$ the
6 source-receiver distance as the approximate depth of the turning point of a ray path, we note that
7 the top 5 km of the model is well covered along the receiver lines. Model depth of 5-20 km is
8 sampled by distributed ray coverage between the two receiver lines, and the coverage of model
9 depths >20 km is sparse.

10

11 2. Checkerboard test

12 Checkerboard tests were conducted using the methods described in [*Zelt, 1998*] and [*Zelt et al.,*
13 2006]. In this test, the final velocity model from the tomography is perturbed by higher and
14 lower velocities, which are added to the final velocity model. The perturbed velocities are
15 imposed in a checkerboard pattern on the model nodes. Synthetic travel times are generated by
16 propagating rays from the sources to the receivers through this checkerboard pattern of perturbed
17 model velocity. These synthetic travel times are inverted in the hope of recovering the
18 checkerboard pattern. The perturbed velocities are $\pm 30\%$ of the given velocity at each model
19 node and are distributed in a 30x30 km size checkerboard pattern of opposite polarities ([Figure](#)
20 [A5](#)). The checkerboard pattern in depth is divided into three layers, 1-10, 10-20, and 20-40 km
21 deep. The synthetic travel-time data uses the same picking error distribution as in the original
22 travel-time data (250 ms for the controlled explosions, 300 ms for the mine explosions and
23 earthquake) and Gaussian noise is added to the synthetic data to simulate realistic picking errors.
24 Similar iterative step method and starting velocity model to the original tomography study are
25 used in the checkerboard tests with the following results.

26

27 (start) RMS = 1231.696 ms (final) RMS = 255.438 ms

28 χ^2 = 19.5266 χ^2 = 0.8819

29

30 Based on the tests, we find that only large-scale features in the velocity model can be resolved
31 (Figure A5) due to the geometry of the shot and receivers. In addition to the areas along the
32 receiver lines in the model, the resolution of the checkerboard is best at the top 2-5 km of the
33 model, where velocity contrasts in the final model are large ($\pm 15\%$) and it decreases with depth,
34 where the velocity contrast is smaller (9-7%). Low velocity areas are difficult to resolve in
35 general in tomography of first-arrival travel time, due to the tendency of the first arrivals to
36 travel through the faster regions of the medium. The resolution of the model seems to be robust
37 enough in the upper 12 km of the model, which is the model region needed to determine the
38 general shape of the Dead Sea basin.

39

40 3. Starting Model test

41 A complement to the checkerboard test is a test of the sensitivity of the final velocity model to
42 different starting velocity models (Table A1). Test Models 1 and 2 are laterally homogenous, but
43 have minor variations compared to the laterally homogenous preferred starting model. Test
44 Models 3 – 7 have different velocities across the transform valley. These velocities are
45 smoothed-out from the 2-D ray-tracing model of the West-East refraction profile (ten Brink et
46 al., 2006; Figure 6a). Identical inversion parameters (travel-time errors, number of iterations,
47 grid cell size, etc.) were used in all the models. Although the goodness of fit of the starting
48 homogenous models (preferred, Test1 and Test 2) is slightly worse than the starting models with
49 lateral variations across the transform valley, the final preferred and Test 1 models fit the
50 observed travel time values as well or better than the other models. The final models with the
51 different starting models all consistently show low and high velocities in the same areas and
52 depths.

53

54 References:

55 Zelt, C. A. (1998), Lateral velocity resolution from three-dimensional seismic refraction data,
56 *Geophysical J. Int.*, 135, 1101-1112.

57 Zelt, C. A., A. Azaria, and A. Levander (2006), 3D seismic refraction travelttime tomography at
58 a ground water contamination site, *Geophysics*, 71, H67-H78.

59

60

61 **Table A1: Model fit to data for inversion with different starting velocities**

Model	Starting RMS (ms) & χ^2		Ending RMS (ms) & χ^2	
Preferred Model	997.462	14.872	521.267	3.932
Test Model 1	1028.586	15.776	525.251	3.994
Test Model 2	921.949	11.658	611.838	5.277
Test Model 3	832.217	9.729	559.190	4.398
Test Model 4	823.063	9.472	561.026	4.429
Test Model 5	844.830	10.399	552.636	4.343
Test Model 6	838.523	10.238	548.836	4.271
Test Model 7	908.325	12.140	589.112	3.932

62

63

64 **Appendix Figure captions**

65 **Figure A1** – (a) Receiver gathers for controlled explosions (panels 1-11). See Table 1 for
66 locations. The gathers were plotted with linear velocity reduction of 7 km/s. Receivers 1 to 409
67 were aligned from south to north and receivers 410 to 755 were aligned from west to east. Red
68 rectangle – enlarged portion of the plot in (b, c). (b, c) Receiver gathers within 100 km of the
69 controlled shots for the north-south and east-west profiles, respectively.

70

71 **Figure A2** – Direct ray paths from controlled explosions 4, 5, and 6, to receivers within the DSB.
72 Note the lack of reciprocity between shots because receiver location was dictated by the
73 availability of roads.

74

75 **Figure A3** - Receiver gathers for controlled explosions (panels 1-11), an earthquake (panel 14)
76 and mining explosions (panels 12-22). See Table 1 for locations. The gathers were plotted with
77 no time reduction. Receivers 1 to 409 were aligned from south to north and receivers 410 to 755
78 were aligned from west to east. Red line – first arrival pick for tomography.

79

80 [Figure A4](#) – Ray path coverage for various shot-receiver distances binned at shot-receiver
81 increments of 20 km. Color dots indicate midpoints for each ray path. Note the uneven coverage
82 due to the locations of all the receivers along two lines (except for a few permanent stations of
83 the Israeli seismic network), and the locations of 14 of the sources at or near these two lines.

84

85 [Figure A5](#) – Depth slices in the checkerboard test. Top - Perturbations in the final velocity model
86 by higher and lower velocities in a checkerboard pattern. Bottom – recovered model. See text for
87 further details.

88

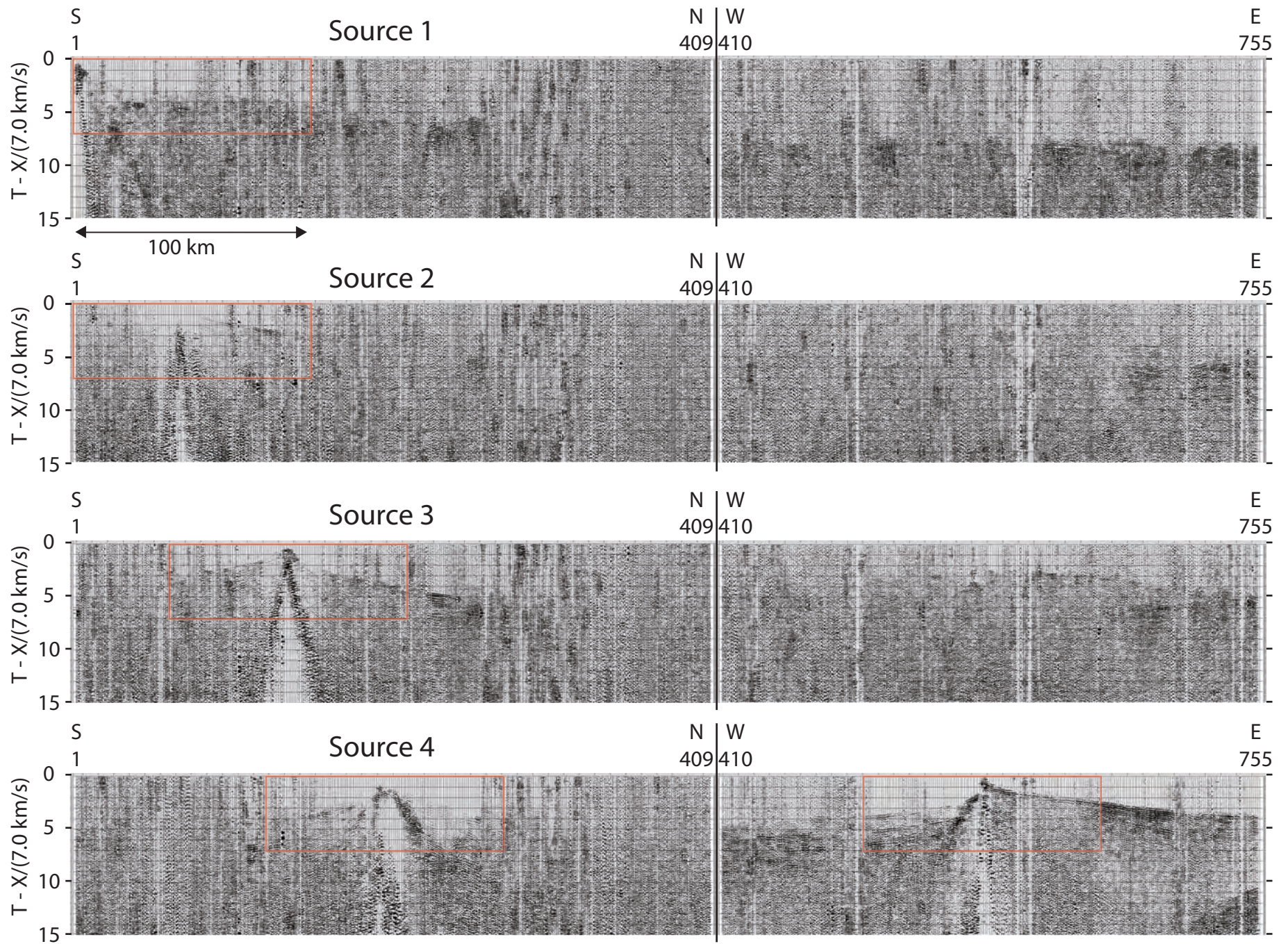
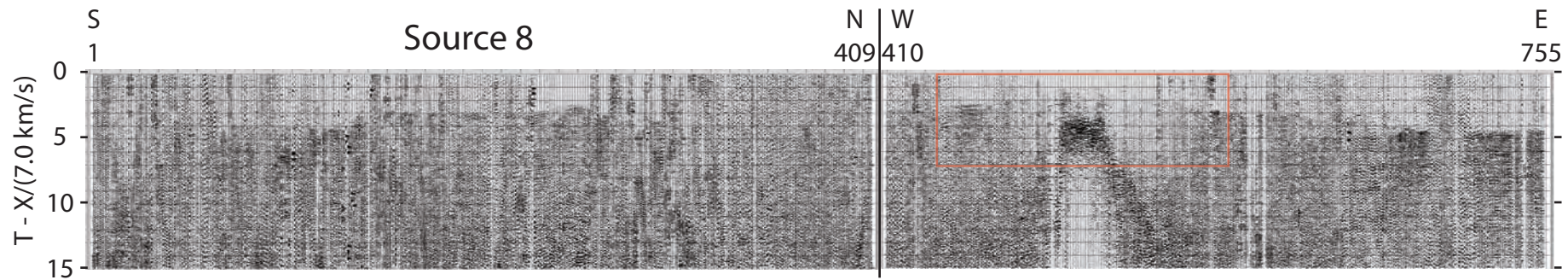
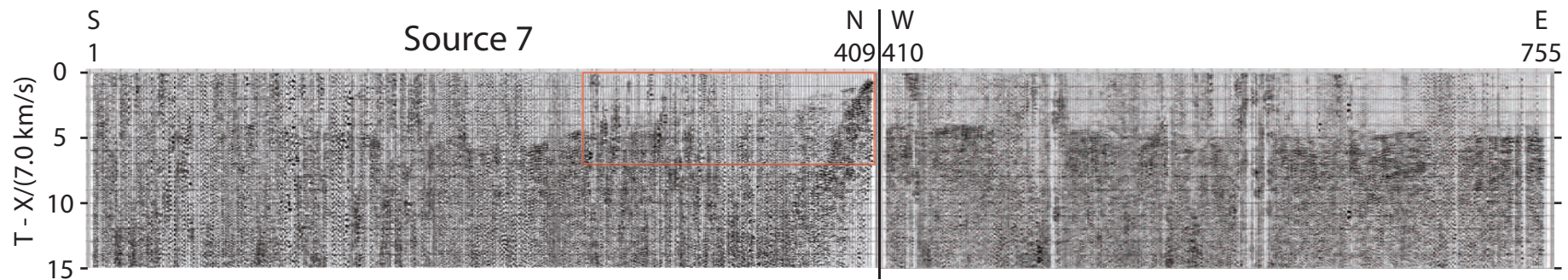
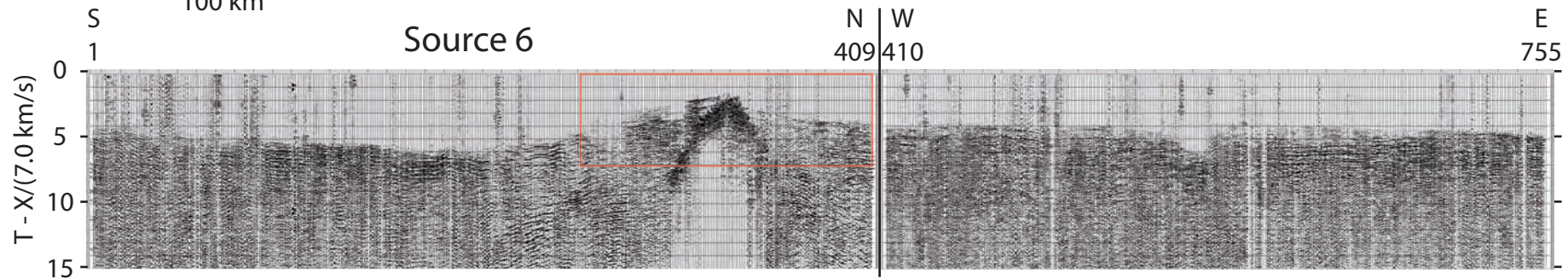
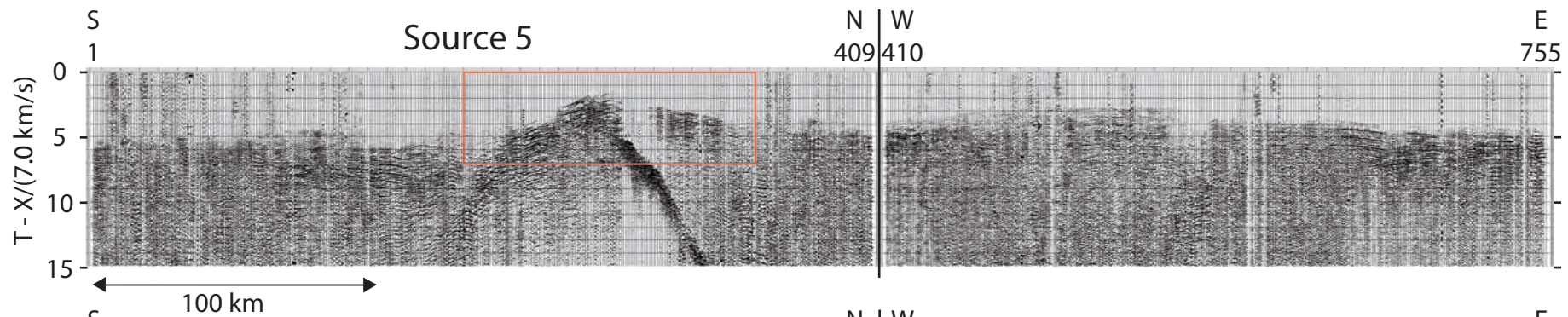
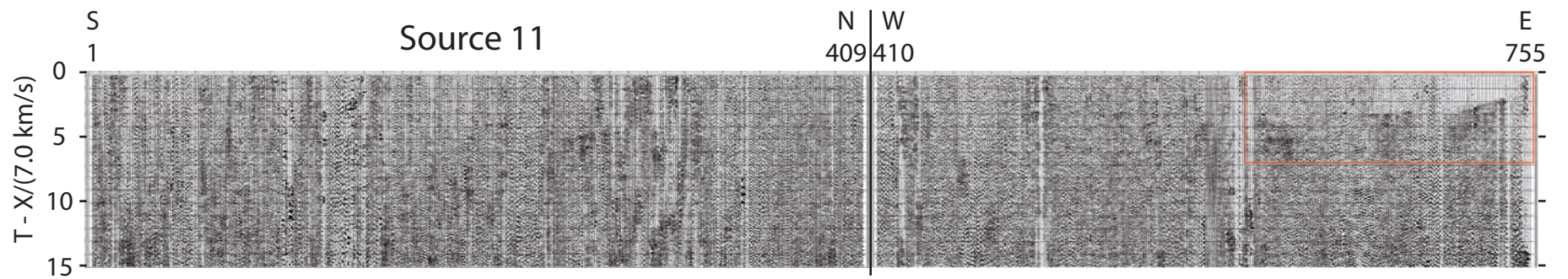
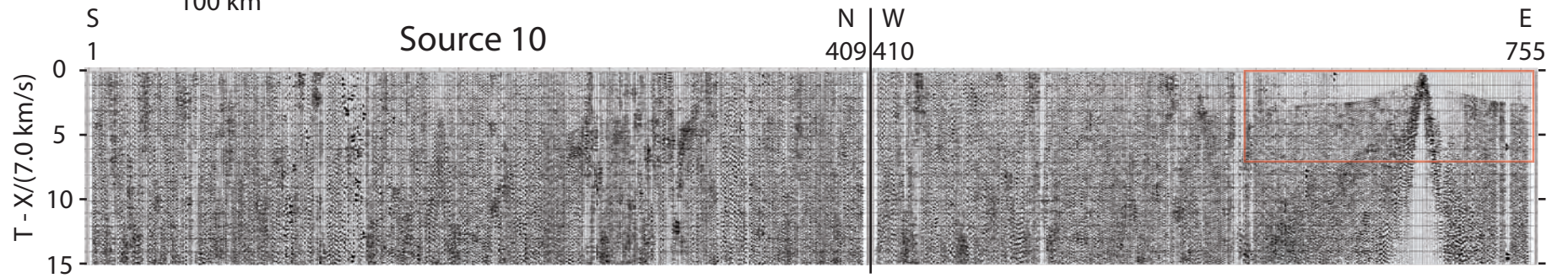
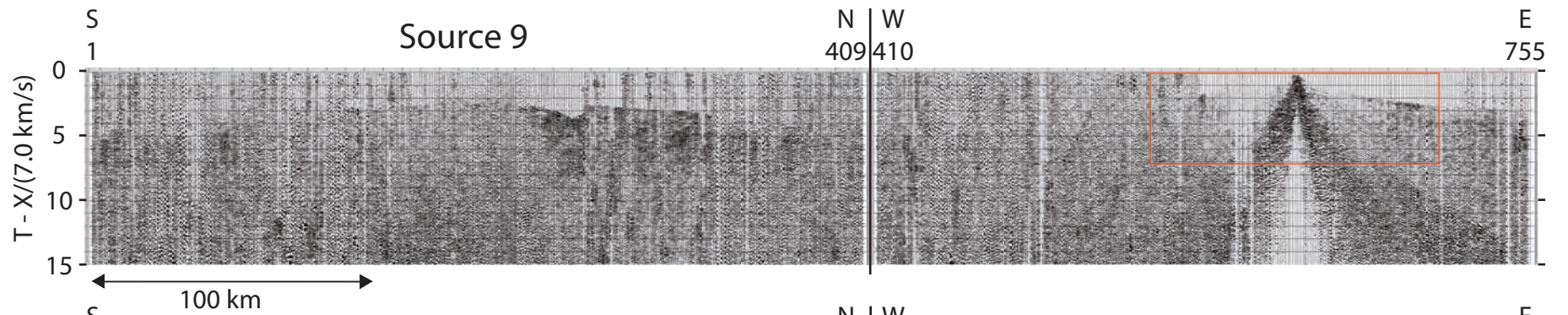


Figure A1a.





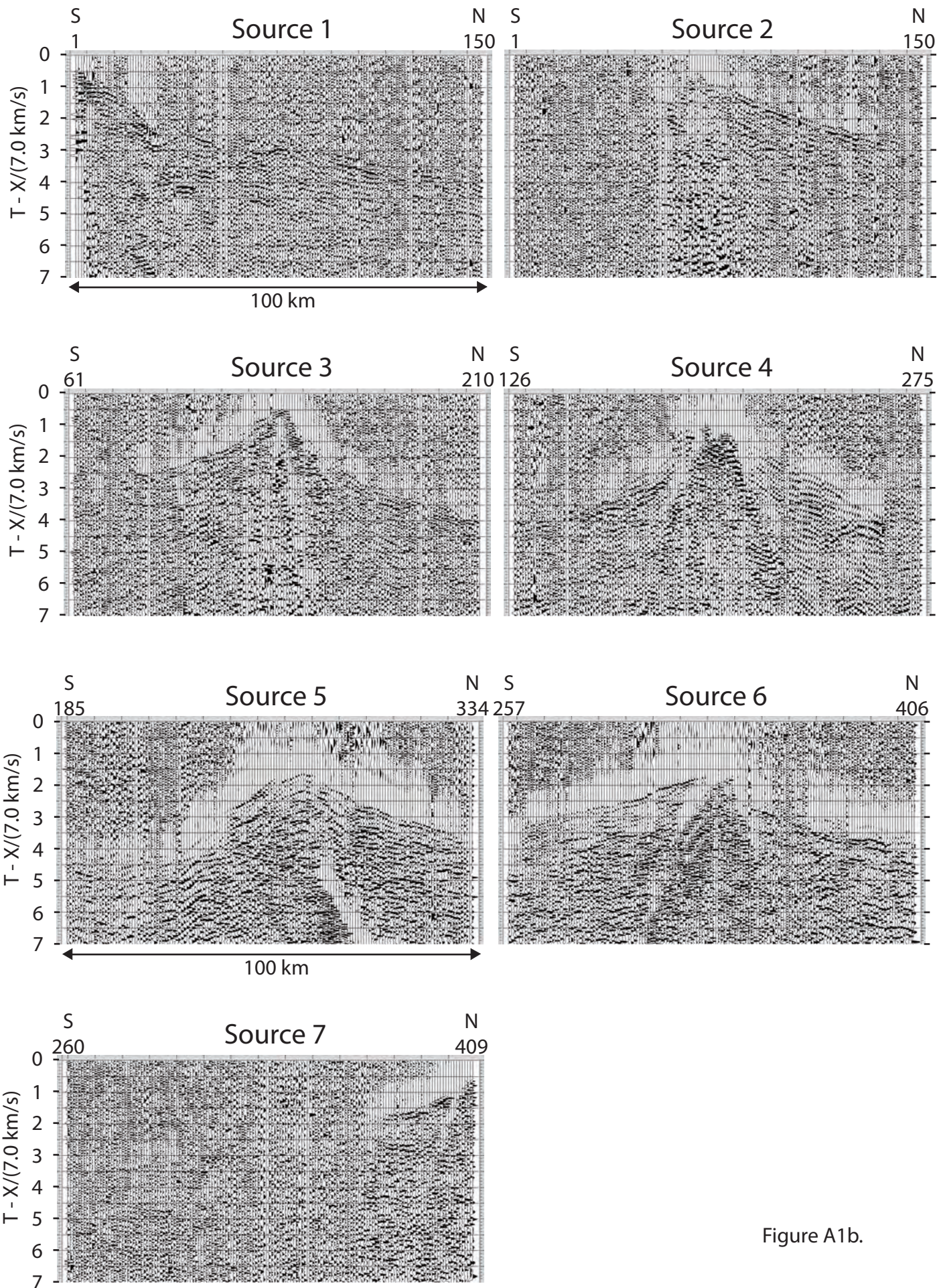


Figure A1b.

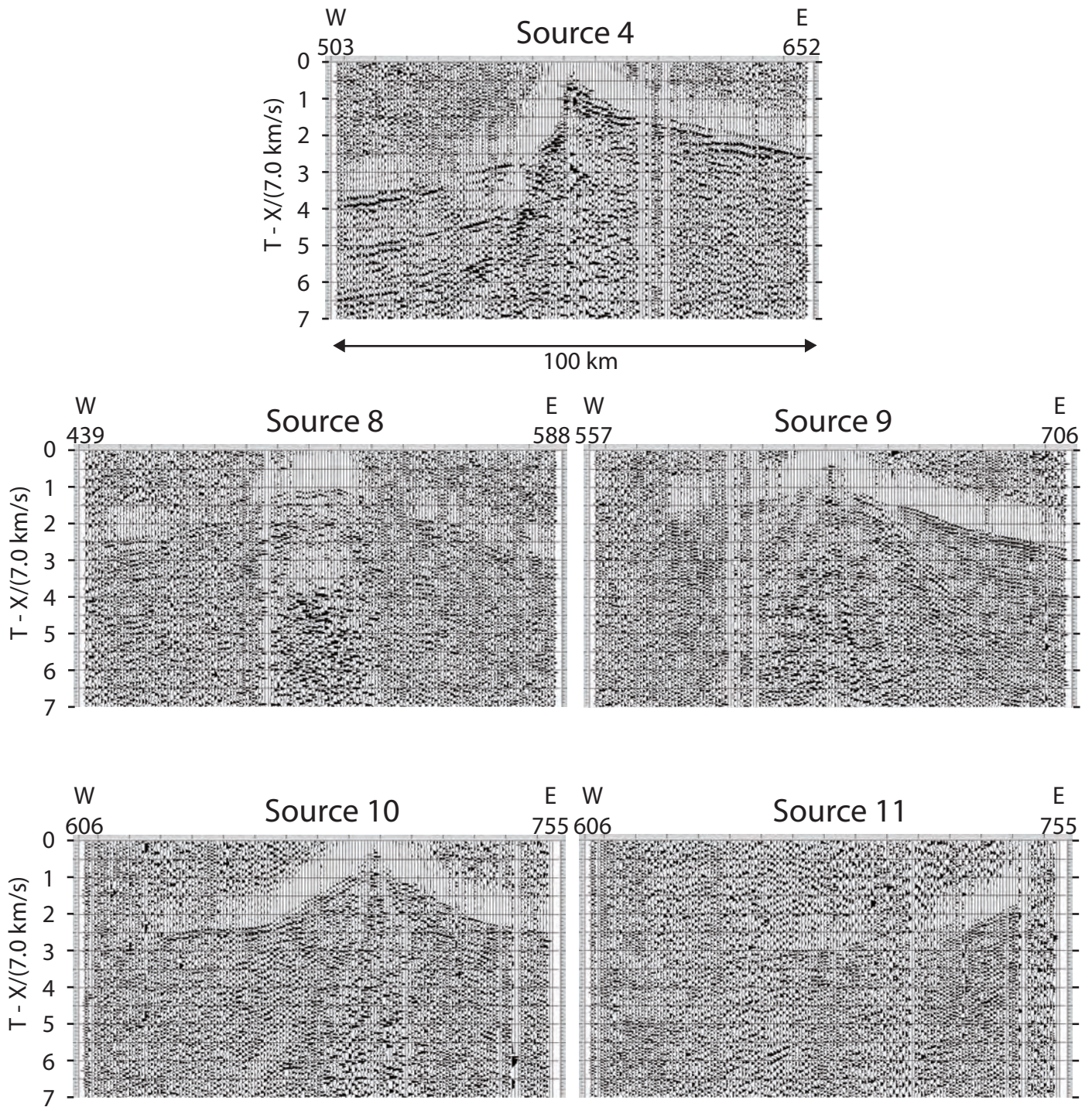


Figure A1c.

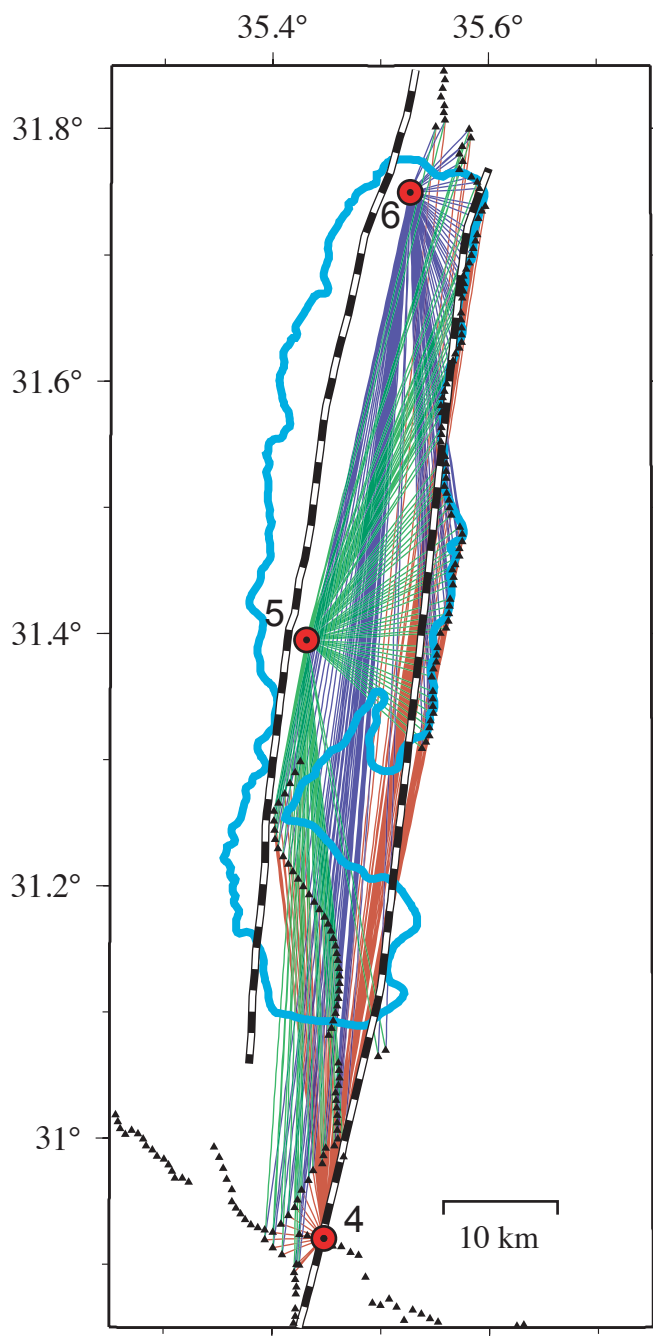


Figure A1.

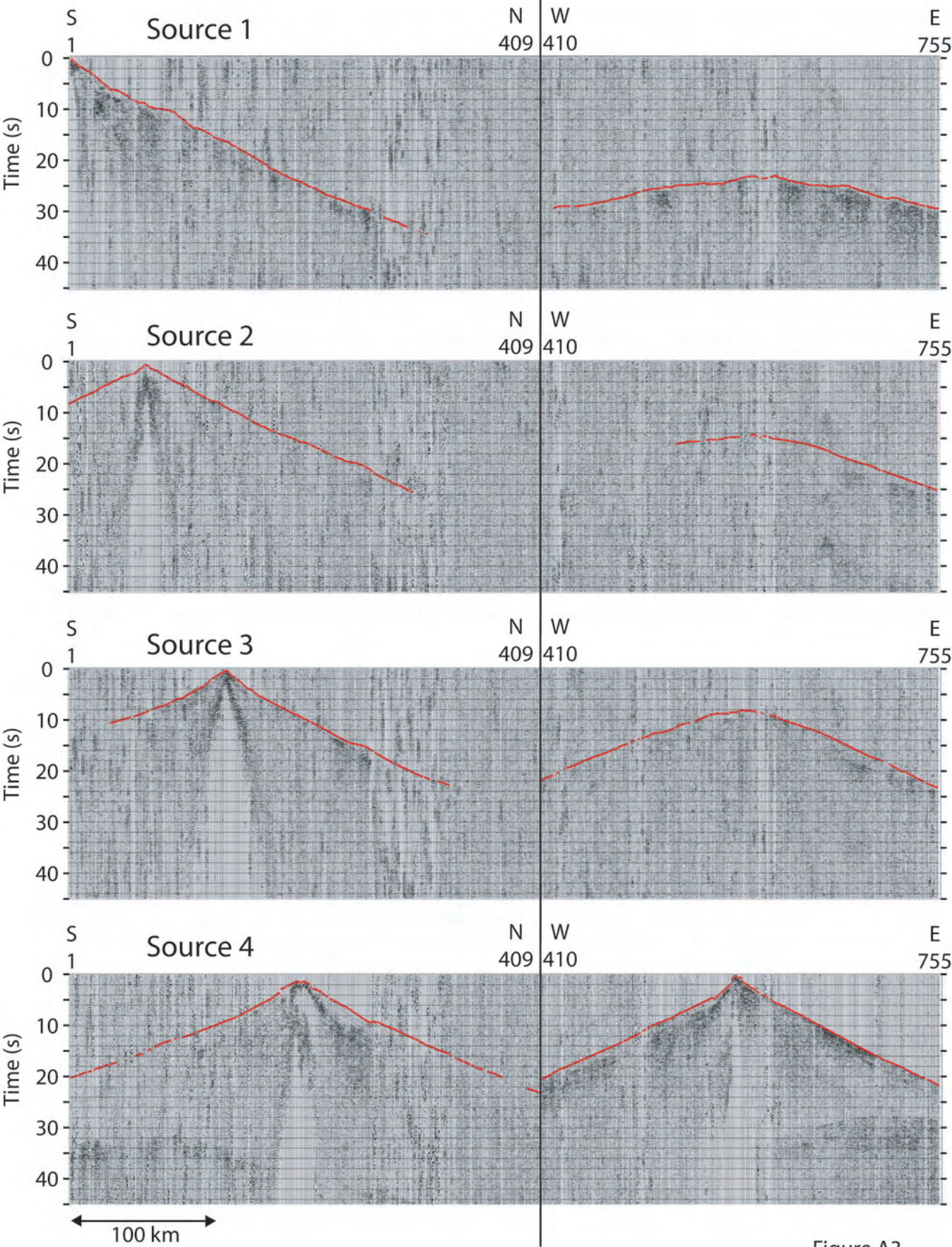
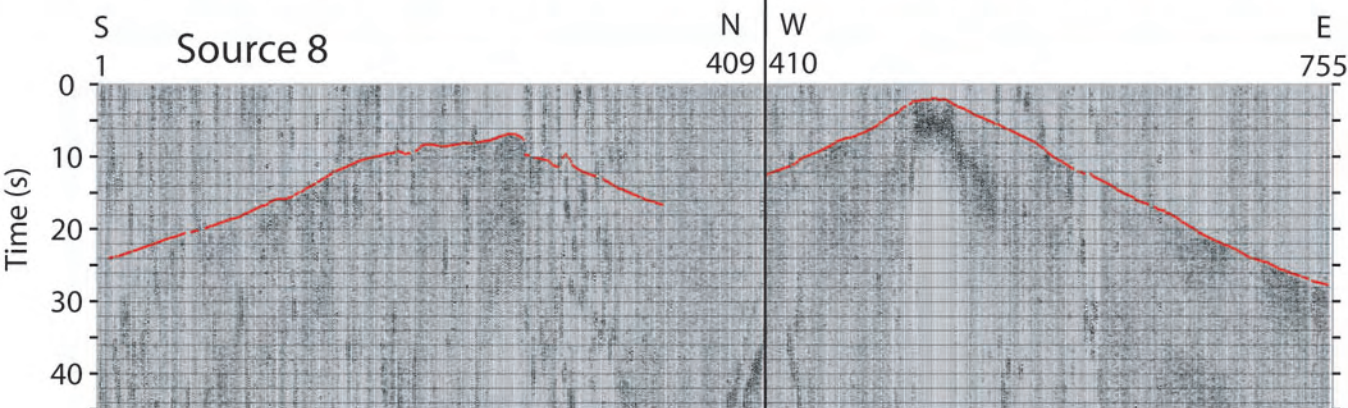
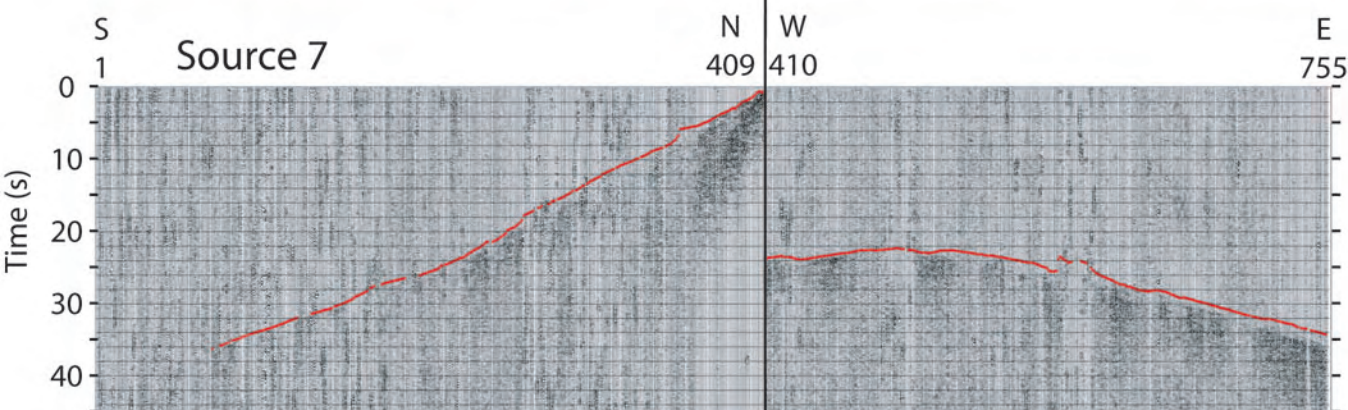
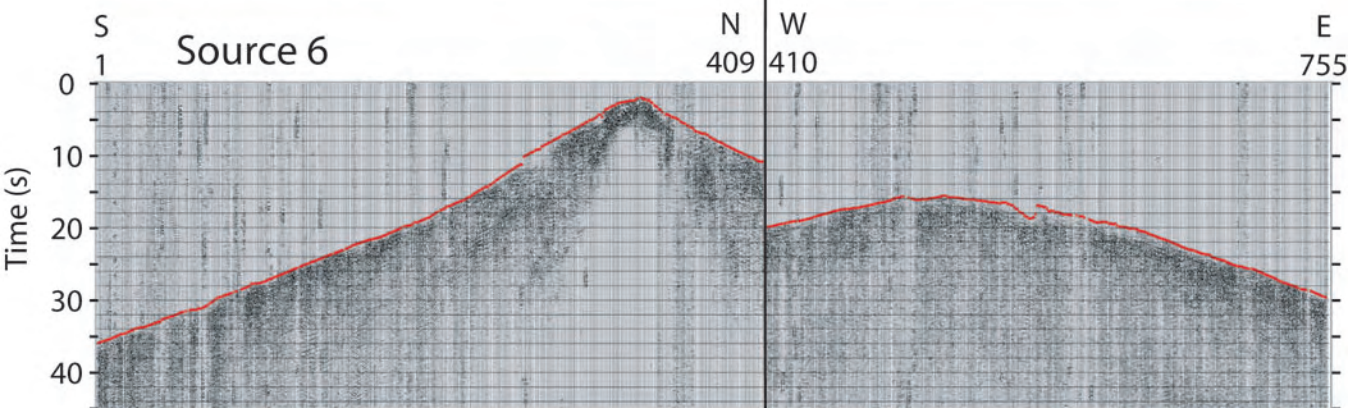
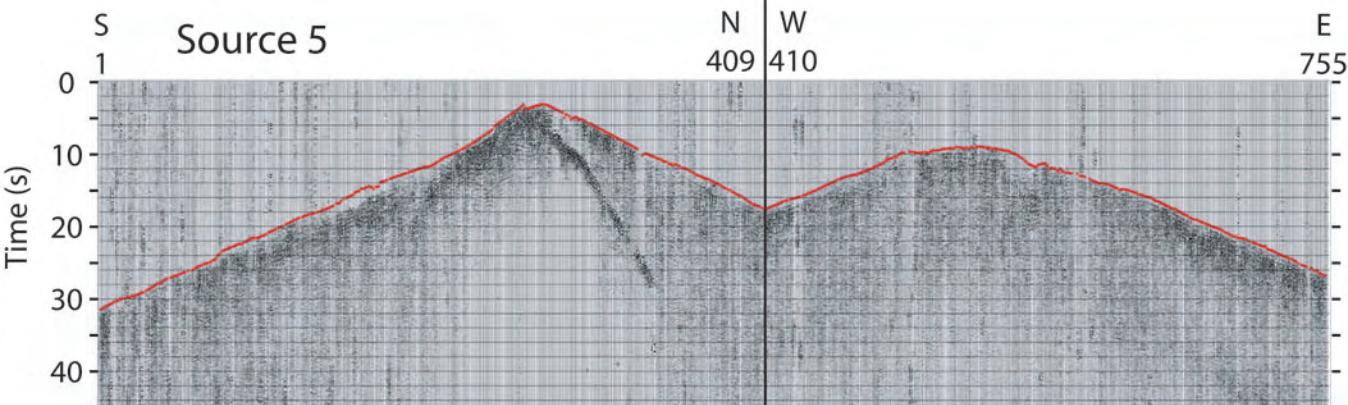
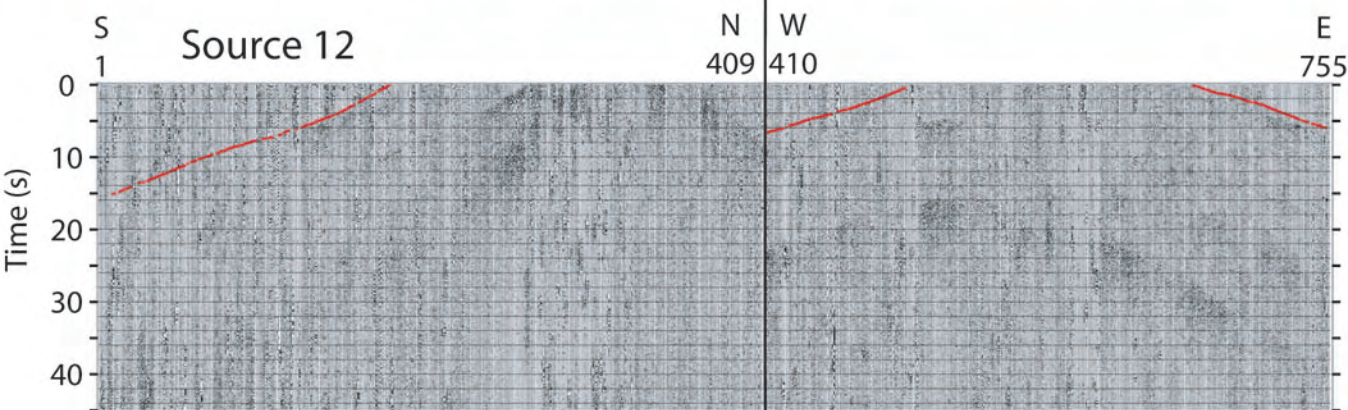
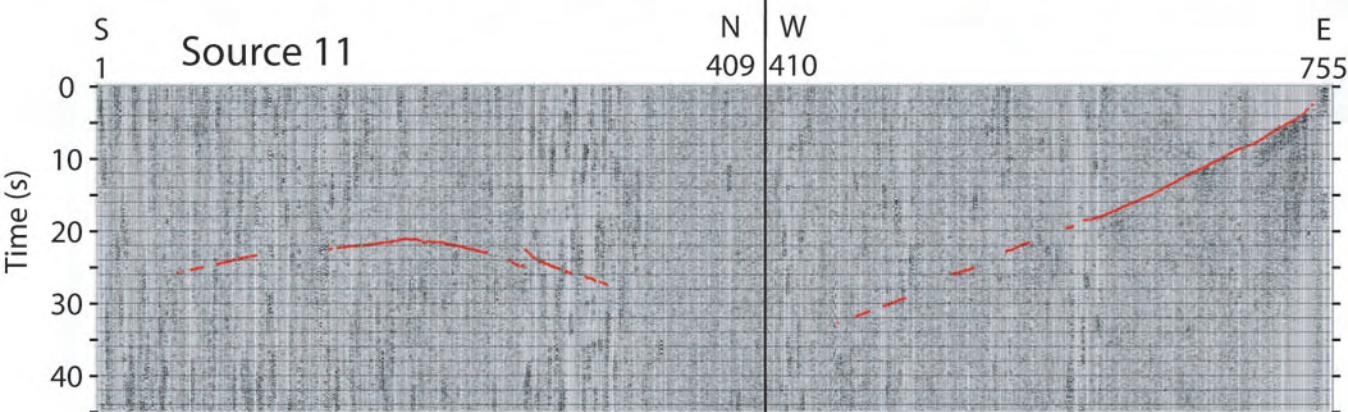
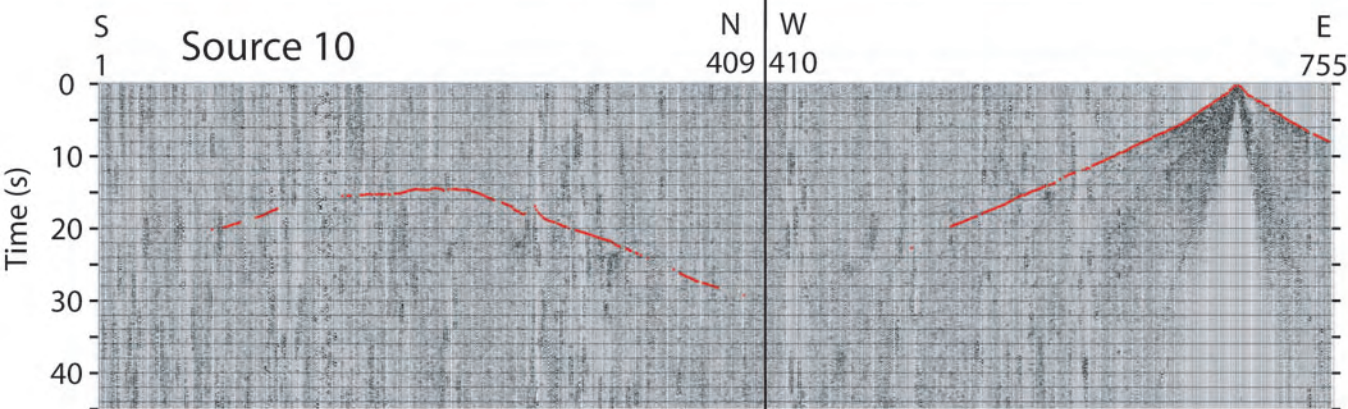
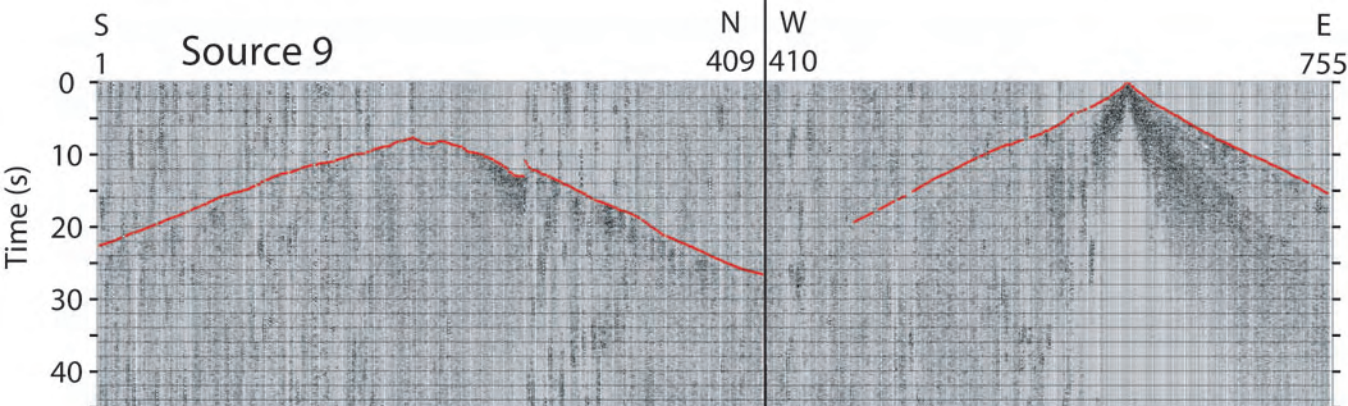


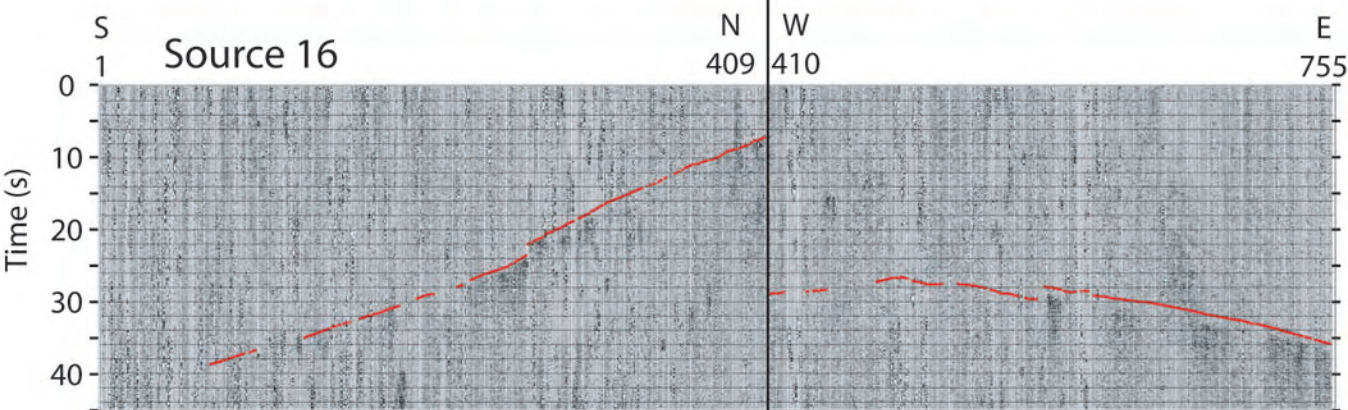
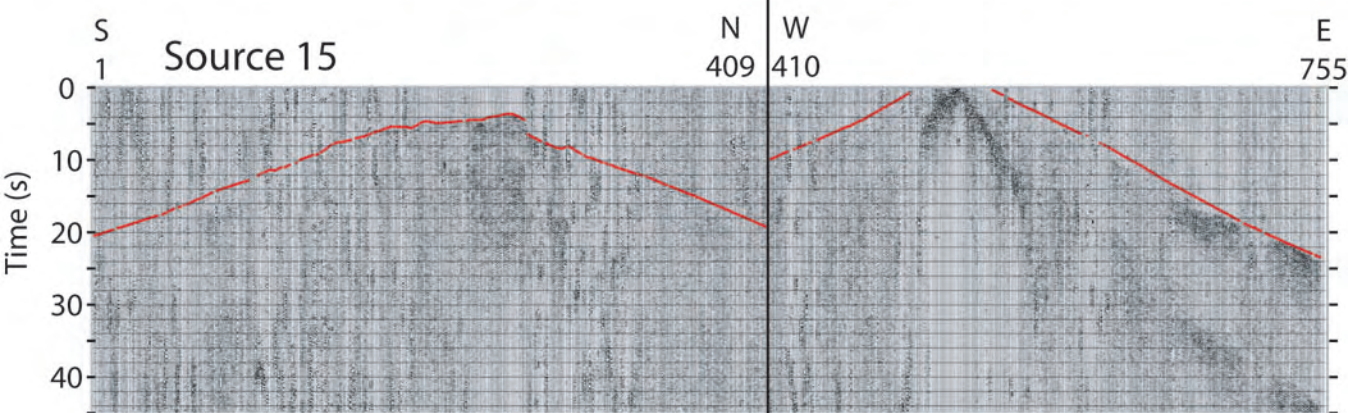
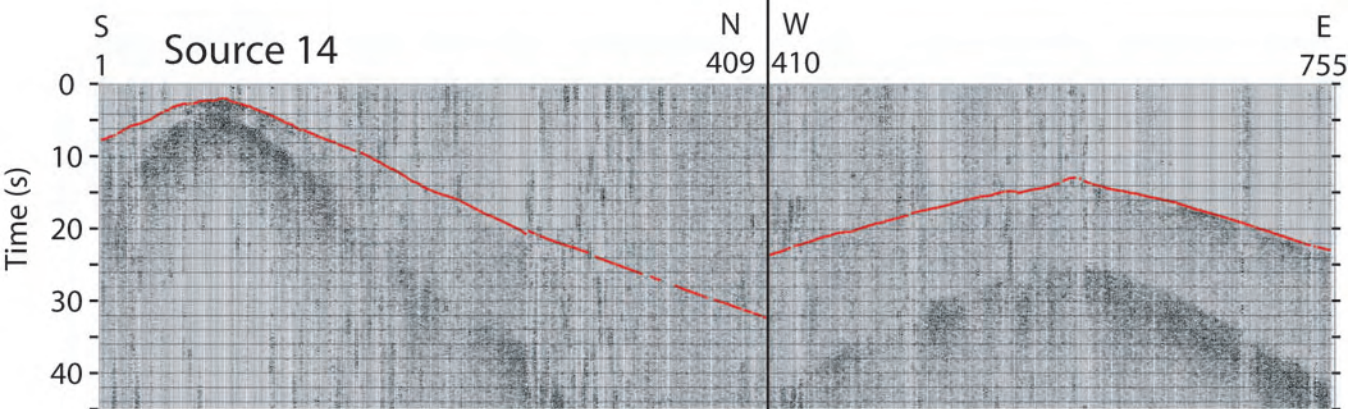
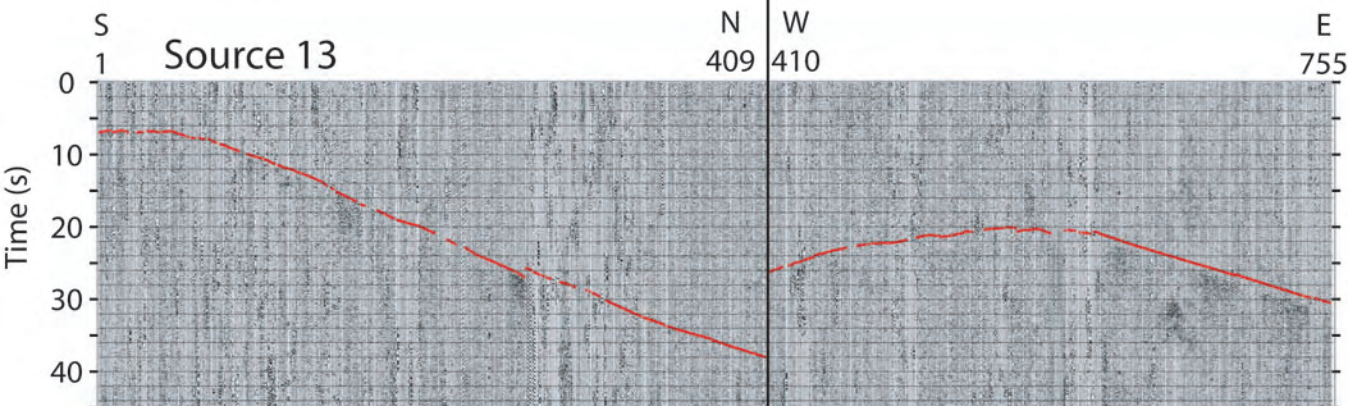
Figure A3



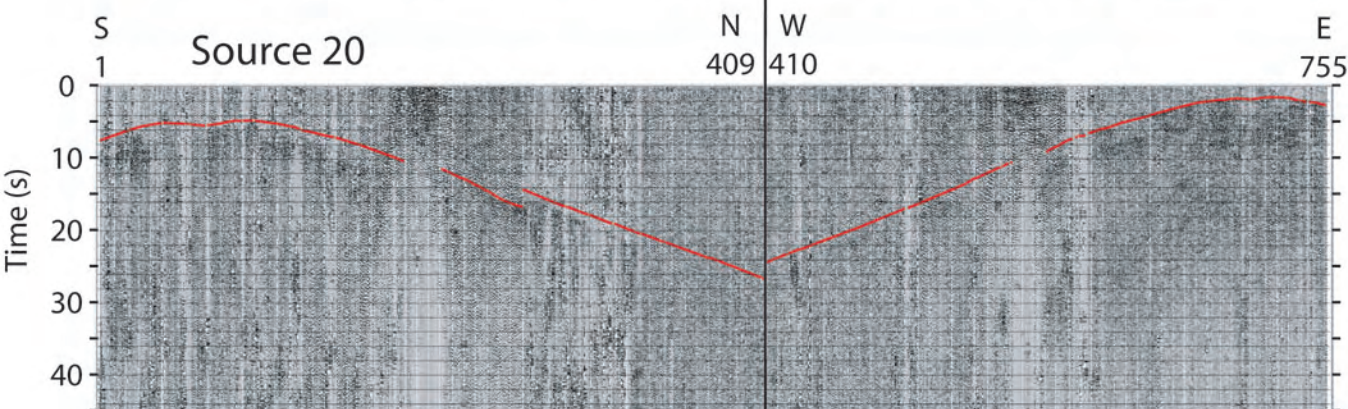
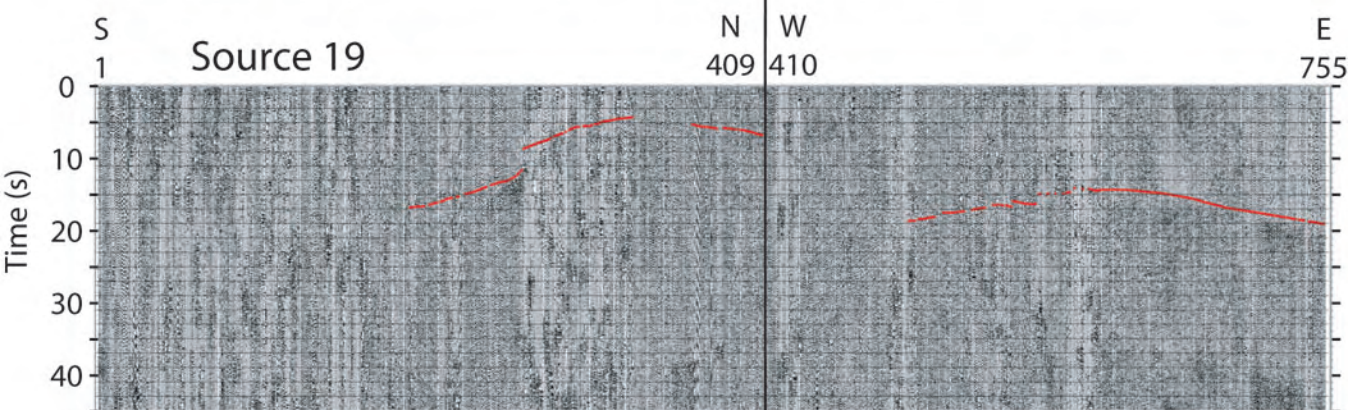
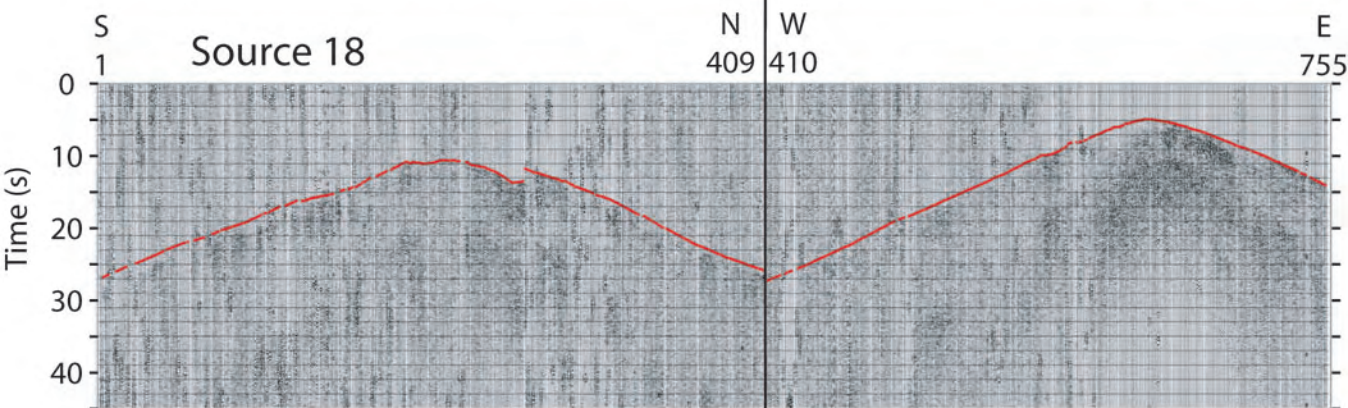
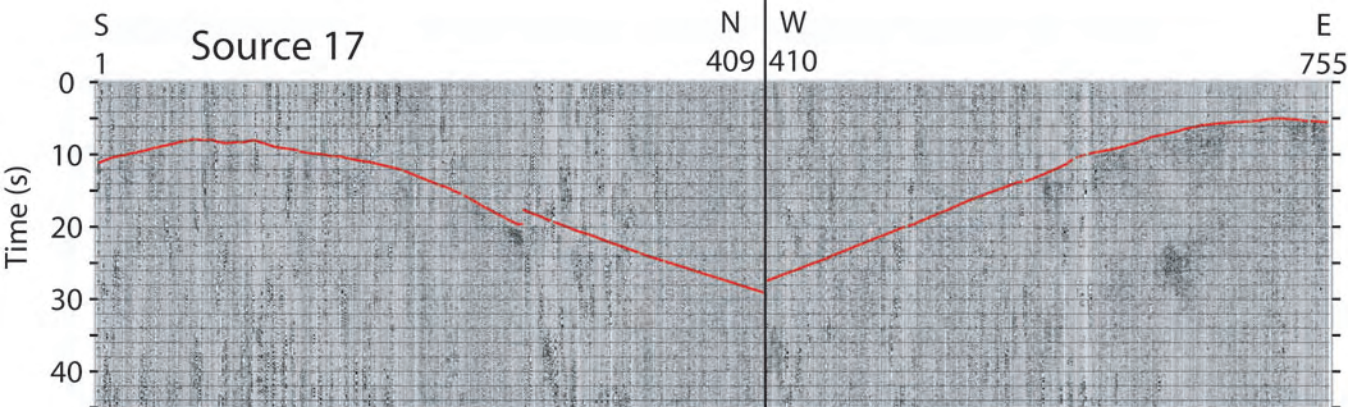
100 km



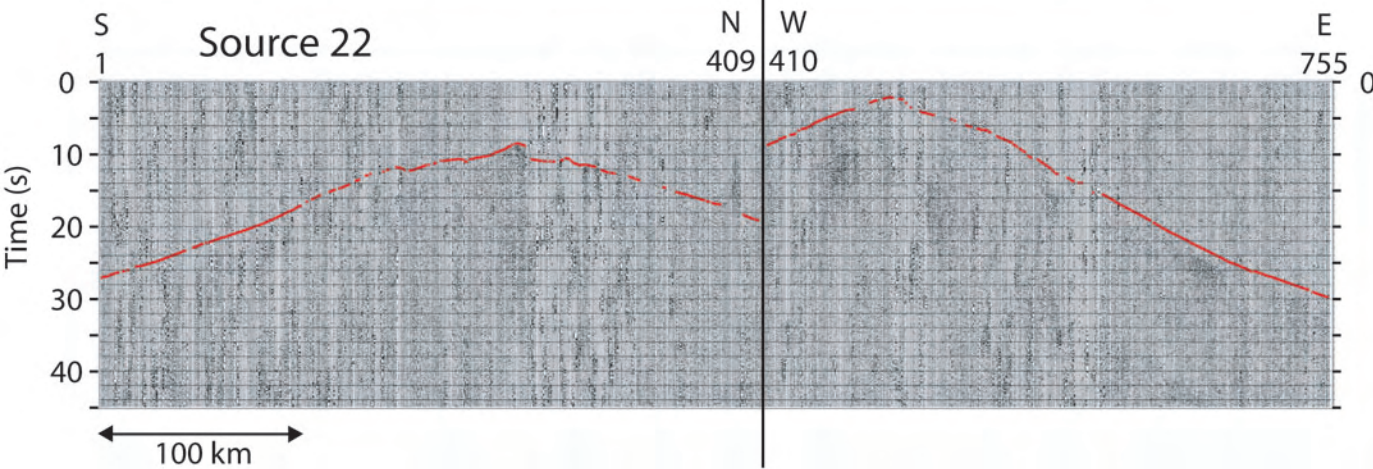
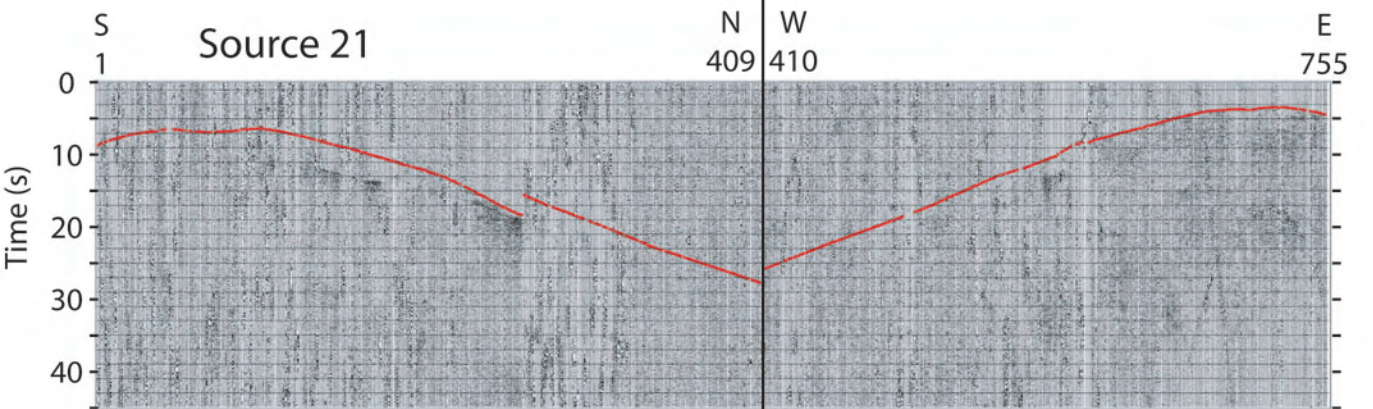
100 km



100 km



100 km



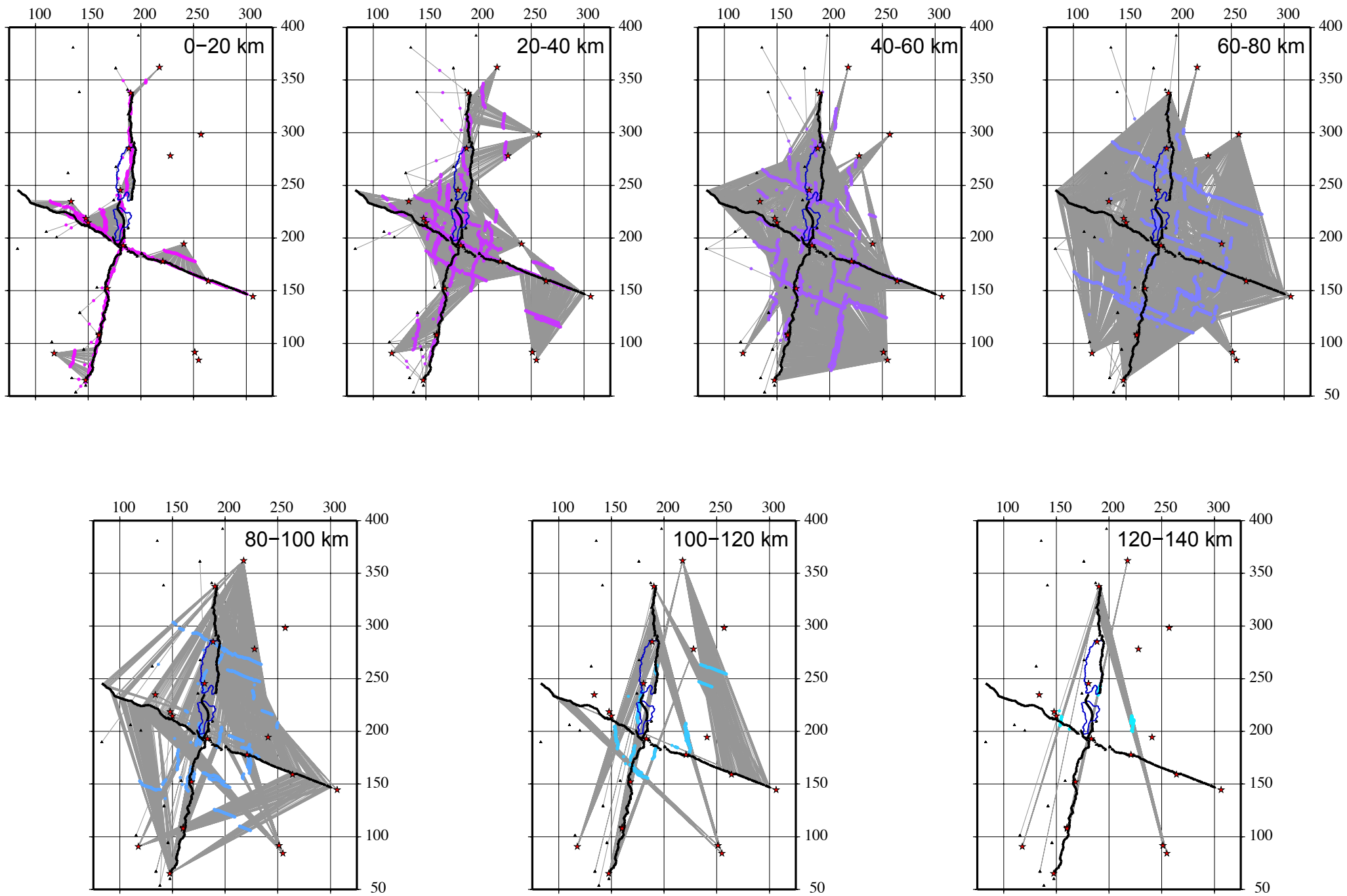


Figure A4.

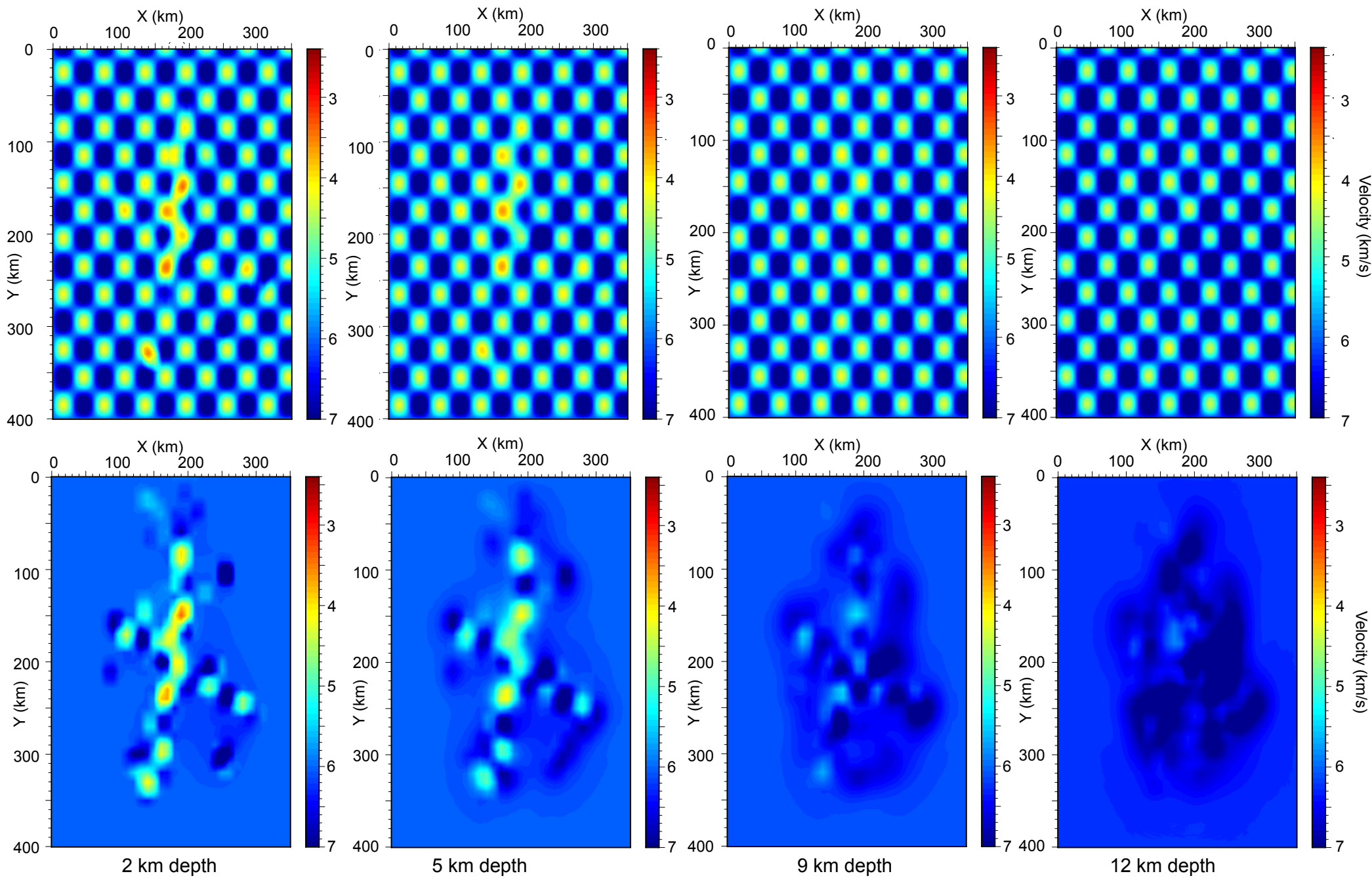


Figure A5.